Impact of the Wiggler Coherent Synchrotron Radiation Impedance on the Beam Instability[*]

Juhao Wu, G.V. Stupakov, T.O. Raubenheimer, Zhirong Huang

Stanford Linear Accelerator Center, Stanford University, Stanford, CA 94309

Abstract

Coherent Synchrotron Radiation (CSR) can play an important role by not only increasing the energy spread and emittance of a beam, but also leading to a potential instability. Previous studies of the CSR induced longitudinal instability were carried out for the CSR impedance due to dipole magnets. However, many storage rings include long wigglers where a large fraction of the synchrotron radiation is emitted. This includes high-luminosity factories such as DAPHNE, PEP-II, KEK-B, and CESR-C as well as the damping rings of future linear colliders. In this paper, the instability due to the CSR impedance from a wiggler is studied assuming a large wiggler parameter K. The primary consideration is a low frequency microwave-like instability, which arises near the pipe cut-off frequency. Detailed results are presented on the growth rate and threshold for the damping rings of several linear collider designs. Finally, the optimization of the relative fraction of damping due to the wiggler systems is discussed for the damping rings.

Submitted to Physical Review Special Topics–Accelerators and Beams

Impact of the Wiggler Coherent Synchrotron Radiation Impedance on the Beam Instability*

Juhao Wu,[†] G.V. Stupakov,[‡] T.O. Raubenheimer,[§] and Zhirong Huang[¶]

Stanford Linear Accelerator Center, Stanford University, Stanford, CA 94309

Coherent Synchrotron Radiation (CSR) can play an important role by not only increasing the energy spread and emittance of a beam, but also leading to a potential instability. Previous studies of the CSR induced longitudinal instability were carried out for the CSR impedance due to dipole magnets. However, many storage rings include long wigglers where a large fraction of the synchrotron radiation is emitted. This includes high-luminosity factories such as DAPHNE, PEP-II, KEK-B, and CESR-C as well as the damping rings of future linear colliders. In this paper, the instability due to the CSR impedance from a wiggler is studied assuming a large wiggler parameter K. The primary consideration is a low frequency microwave-like instability, which arises near the pipe cut-off frequency. Detailed results are presented on the growth rate and threshold for the damping rings of several linear collider designs. Finally, the optimization of the relative fraction of damping due to the wiggler systems is discussed for the damping rings.

I. INTRODUCTION

When an electron bunch passes the curved trajectory inside a dipole, the coherent synchrotron radiation (CSR) induces an impedance [1–4]. The CSR impedance is known to impact single pass bunch compressors where the beam currents are extremely high [5–8] but it is also possible that CSR might cause a microwave-like beam instability in storage rings. A theory of such an instability in a storage ring has been recently proposed in Ref. [9] where the impedance is generated by the synchrotron radiation of the beam in the storage ring bending magnets.

A similar instability may arise due to coherent synchrotron radiation in long wigglers. Many storage rings have used large wiggler systems to reduce the damping times and control the beam emittance. In particular, the high luminosity colliding beam factories DAPHNE [10], PEP-II [11], KEK-B [12], CESR-C [13] all have wiggler systems that can radiate significantly more power than is radiated in the arc bending magnets. Similarly, damping ring designs for future linear colliders rely on large wiggler systems to obtain the required damping rates where, again, more power can be radiated in the wiggler systems than in the arc bending magnets.

In a previous study, the wakefield and impedance in a wiggler with large parameter K has been obtained [14] based on the work of Saldin *et al.* [15]. In this paper, we study the impact of the wiggler synchrotron radiation impedance on the beam longitudinal dynamics in rings with dipoles and wigglers. We focus our attention on the limit of a large wiggler parameter K because this is the most interesting case for many applications.

The paper is organized as follows. In Sec. II, we will briefly review the theory of the beam instability in a ring due to the CSR impedance [9]. Using the synchrotron radiation impedance of a wiggler [14], we study the beam instability problem for a ring including both dipoles and wigglers in Sec. III. In Sec. IV, we then focus on a low-frequency microwave-like CSR instability near the pipe cut-off frequency which is the primary limitation. Finally, in Sec. V, we discuss effect of the CSR instability on the design optimization of damping rings for future linear colliders. Finally, we give some discussions and conclusion in Sec. VI.

II. LONGITUDINAL BEAM INSTABILITY

We consider the longitudinal dynamics of a thin coasting beam. The beam can be described with a longitudinal distribution function $\rho(\nu, s, z)$. The positive direction for the internal coordinate s is pointing to the direction of the motion. The relative energy offset of a particle having energy E with respect to the nominal energy E_0 is expressed as $\nu = (E - E_0)/E_0$. The position of the reference particle in the beam line is $z = c\,t$ with c equal to the speed of light in vacuum.

The longitudinal beam instability due to the synchrotron radiation impedance in a ring has been studied theoretically by Stupakov and Heifets [9]. In this section, we briefly review and reproduce the equations we need for our study in this paper. The reader is advised to refer to reference [9] for the details of the theory.

For a matched beam, one can use a 1-D Vlasov equa-

---

tion to describe the evolution of the longitudinal distribution function $\rho(\nu, s, z)$.

$$
\begin{aligned}
0 = & \frac{\partial \rho}{\partial z} - \eta \nu \frac{\partial \rho}{\partial s} \\
& - \frac{r_0}{\gamma} \frac{\partial \rho}{\partial \nu} \int_{-\infty}^{\infty} d\nu' \int_{-\infty}^{s} ds' \, w(s - s') \, \rho(\nu', s', z) \, , \quad (1)
\end{aligned}
$$

where, the slippage factor is defined as

$$
\eta = \alpha - \frac{1}{\gamma^2} \, , \quad (2)
$$

with α equal to the momentum compaction factor. For ultrarelativistic beams, we have $\eta \approx \alpha$. Based on our definition of s, the sign convention for α is then the following. If a particle with a higher energy than the nominal energy, i.e., $\nu > 0$, would go to the head of the bunch, then the beam line provides a negative α. According to this convention, then in a simple bending magnet, we will have $\alpha > 0$, while in a wiggler, we have $\alpha < 0$.

The distribution function ρ is written as a sum of the equilibrium distribution function and a perturbation, $\rho = \rho_0(\nu) + \rho_1(\nu, s, z)$, with $\rho_1 \ll \rho_0$. We look for a perturbation as

$$
\rho_1 = \hat{\rho}_1 \, e^{-i \omega z/c + i k s} \, , \quad (3)
$$

where k is the wavenumber, ω the frequency. Linearizing the 1-D Vlasov Eq. (1) leads to the dispersion relation [9]:

$$
1 = \frac{i \, r_0 \, c \, Z(k)}{\gamma} \int_{-\infty}^{\infty} d\nu \frac{d\rho_0/d\nu}{\omega + c \, k \, \eta \, \nu} \, , \quad (4)
$$

which determines the existence of a solution as in Eq. (3). Here, $r_0 \approx 2.82 \times 10^{-15}$ m is the classical electron radius and γ is the Lorentz factor. In addition,

$$
Z(k) = \int_0^{\infty} ds \, w(s) \, e^{-i k s} \, , \quad (5)
$$

is the CSR impedance and the wake Green function $w(s)$ describes the interaction of two particles due to the synchrotron radiation where $w(s) \neq 0$ for $s > 0$ while $w(s) = 0$ for $s < 0$. The positive values of $w(s)$ correspond to the energy loss and the negative values imply the energy gain.

We assume that the initial energy distribution function is a Gaussian, i.e., $\rho_0 = n_0/(\sqrt{2\pi} \, \nu_0) \times \exp(-\nu^2/2 \, \nu_0^2)$, where n_0 is the linear density, i.e., the number of particles per unit length. In this case, Eq. (4) can be rewritten as,

$$
1 = -\frac{i \, Z(k) \, \Lambda}{\sqrt{2\pi} \, k} \int_{-\infty}^{\infty} dp \frac{p \, e^{-\frac{p^2}{2}}}{\Omega \pm p} \quad (6)
$$

where, $\Lambda = n_0 \, r_0/(|\eta| \, \gamma \, \nu_0^2)$; $\Omega = \omega/(c \, k \, |\eta| \, \nu_0)$ and $p = \nu/\nu_0$. The upper (lower) sign in Eq. (6) refers to the case of a positive (negative) η. We refer the reader to Ref. [9] for further details.
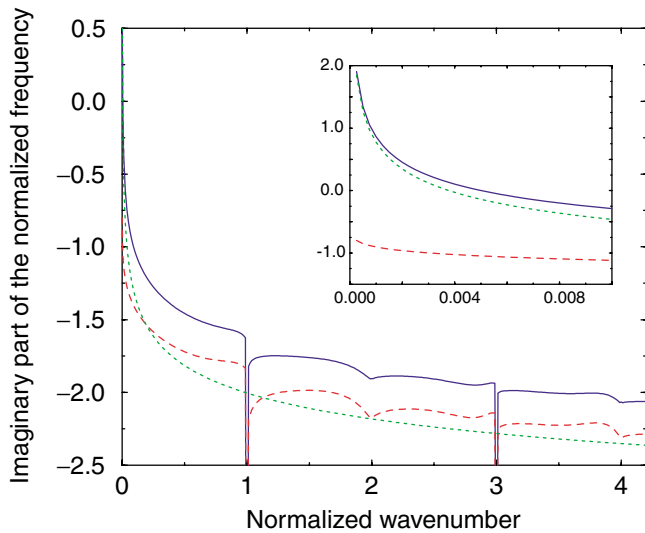

FIG. 1: The imaginary part of the normalized frequency Ω as a function of the normalized wavenumber k/k_0 for the NLC main damping ring [16] where k_0 is the on-axis wiggler fundamental radiation wavenumber defined in Eq. (14). The solid curve includes the entire CSR impedance while the dotted and dashed curves include either the steady state dipole CSR impedance or the wiggler CSR impedance, respectively. The inset shows a blow up of the low frequency region where the beam is unstable.

III. STORAGE RINGS WITH WIGGLERS

As mentioned, a number of storage rings utilize long damping wigglers where a significant fraction of the energy loss per turn is emitted. As concrete examples, we study the NLC main damping ring [16], the TESLA damping ring [17], and the KEK ATF prototype damping ring [18]. Parameters are given in Table I.

In our paper, we use the steady state CSR impedance and assume a distributed impedance model. For a dipole, the steady state CSR impedance is [1, 2]

$$
Z_D(k) = -i \, A \, \frac{k^{1/3}}{R^{2/3}} \, , \quad (7)
$$

with

$$
A = 3^{-1/3} \, \Gamma\left(\frac{2}{3}\right) (\sqrt{3} \, i - 1) \, . \quad (8)
$$

The wiggler impedance $Z_W(k)$ is computed in Ref. [14]. Hence, the total impedance is then

$$
Z(k) = Z_D(k) \frac{\Theta \, R}{C} + Z_W(k) \frac{L_W}{C} \, , \quad (9)
$$

where, R, Θ, L_W and C are the dipole bending radius, the total bending angle, the wiggler total length and the damping ring circumference given in Table I respectively.

To study the instability, we numerically solve the dispersion relation Eq. (6). Since we are assuming a coasting beam model, we only consider instability wavelengths short compared to the bunch length.

	NLC	TESLA	ATF
Circumference C/km	0.3	17	0.14
Dipole radius R/m	5.5	80	5.7
Total bending angle $\Theta/2\pi$	1	5/3	1
Momentum compaction $\alpha/10^{-4}$	2.95	1.2	19
Synchrotron frequency Q_s/kHz	3.5	0.8	17.4
Extracted X emittance $\gamma\epsilon_x/10^{-6}$m	3	8	5
Extracted Y emittance $\gamma\epsilon_y/10^{-8}$m	2	2	5
Energy E/Gev	1.98	5	1.3
Energy rms spread $\nu_0/10^{-4}$	9.09	9	6
Bunch rms length σ_z/mm	3.6	6	5
Particles in a bunch $N_e/10^{10}$	0.75	2	1
Wiggler peak field B_w/T	2.15	1.5	1.88
Wiggler period λ_w/m	0.27	0.4	0.4
Wiggler total length L_w/m	46.24	432	21.2
Wiggler β-function $\beta_{x,w}$/m	1.87	6.67	6
Pipe radius b/cm	1.6	2	1.2
F_w	2.2	13.4	1.8
Cut-off wavelength λ_c/mm	4.9	1.8	3.1
Threshold at cutoff (wiggler off) $N_t/10^{10}$	0.60	27.44	0.95
Threshold at cutoff (wiggler on) $N_t/10^{10}$	0.52	24.56	0.76
Growth time at cutoff (wigger off) $\tau/\mu s$	54.9	N/A	34.3
Growth time at cutoff (wigger on) $\tau/\mu s$	32.9	N/A	6.5

TABLE I: Parameters and results for the NLC main damping ring [16], the TESLA damping ring [17], and the KEK ATF prototype damping ring [18]. The parameter F_w is the ratio of the radiation power emitted in the wiggler to that emitted in the arc bending magnets defined in Eq. (16).

In Fig. 1, the imaginary part of Ω is plotted as a function of the instability wavenumber for the NLC main damping ring using the parameters listed in Table I. At low frequencies, the dipole CSR impedance dominates while at shorter wavelengths the wiggler CSR impedance is usually more important. In the region where Im(Ω)< 0, the beam is stable and this is true for all regions except at the longest wavelengths as shown in the inset. This low frequency instability will be discussed in the following section.

Similar calculations were made for the TESLA "dog-bone" damping ring, where the total bending angle is about $\Theta = 10\pi/3$, and the KEK ATF prototype damping ring. For the design current in the TESLA damping ring, the impedance from the dipoles and wigglers will not drive an instability while the results for the ATF are very similar to those of the NLC damping ring shown in Fig. 1.

One interesting effect can be seen at the wiggler radiation fundamental frequency and the odd harmonics where the ring is actually stabilized by the wiggler impedance. This is opposite to the single-pass behaviour through a wiggler where there is an instability at the wiggler fundamental frequency usually refered to as the FEL instability. The effect will be discussed further in Appendix A

but is a direct result of the positive sign of the momentum compaction in the ring.

To illustrate this, Fig. 2 is a plot for the NLC damping ring with identical wiggler and arc parameters but the momentum compaction is assumed to be opposite in sign. Here, one can see that at low frequencies the growth is slightly lower. In contrast, the wiggler impedance makes the system less stable at the wiggler fundamental unlike the case with positive momentum compaction. Furthermore, if the magnitude of the momentum compaction is reduced, the system will become unstable similar to that illustrated in Appendix B. This is similar to the FEL instability however, it is also noted in Appendix A that our theory does not correctly treat the full FEL instability.

IV. LOW-FREQUENCY CSR INSTABILITY

As seen in Figs. 1 and 2, the instability is most important at relatively low frequency. The longest instability wavelength that is possible is determined by two effects: first, the instability wavelength has to be short compared to the bunch length and, second, the vacuum chamber causes an exponential suppression of the synchrotron radiation at wavelengths λ greater than the 'shielding cut-
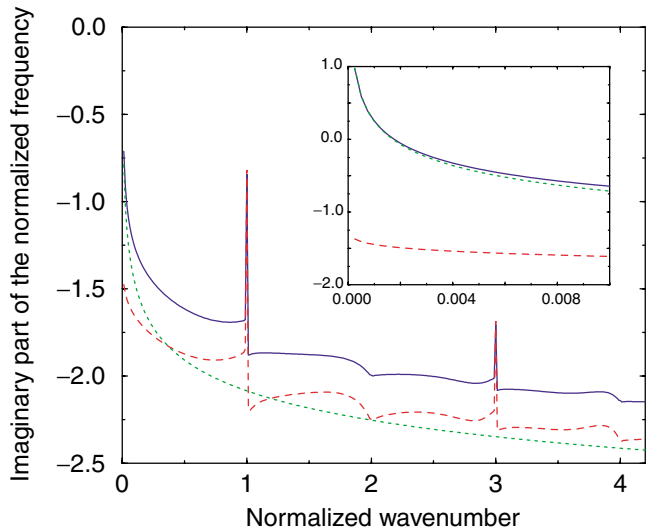
FIG. 2: The imaginary part of the normalized frequency Ω as a function of the normalized wavenumber k/k_0 for the NLC main damping ring with negative momentum compaction where k_0 is the on-axis wiggler fundamental radiation wavenumber defined in Eq. (14). The solid curve includes the entire CSR impedance while the dotted and dashed curves include either the steady state dipole CSR impedance or the wiggler CSR impedance, respectively. The inset shows a blow up of the low frequency region where the beam is unstable.
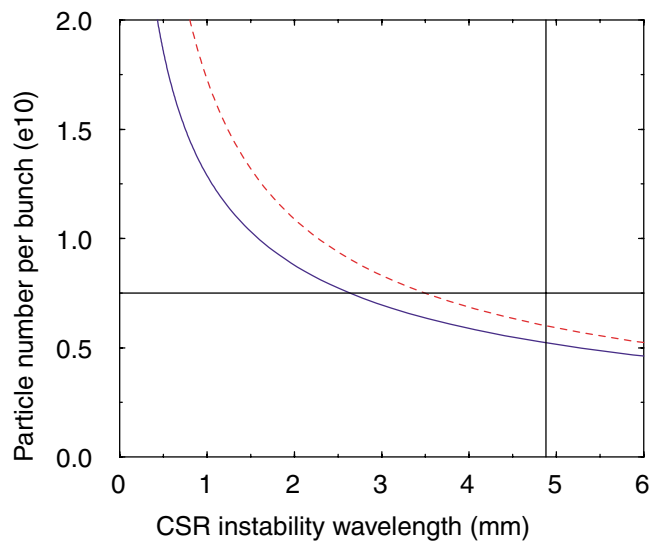

FIG. 3: The threshold particle number as a function of the CSR wavelength for the NLC main damping ring. The dashed curve is the result for the dipoles only, while the solid curve takes into account of the contributions from the dipoles and the wigglers. The vertical straight line is the approximate cutoff wavelength according to Eq. (10). The horizontal straight line is the nominal number of particles per bunch: 0.75×10^{10}.

off' [3]

$$\lambda_c \leq 4\sqrt{2}b(b/R)^{1/2} \ . \tag{10}$$

Here, R is the dipole bending radius, and b is the vacuum chamber half height. The numerical coefficient of Eq. (10) assumes that the vacuum chamber is made up of two infinitely wide plates. Different cross sections give different numerical factors [23]. Given the previous discussion, the threshold will be the lowest at the smaller of the bunch length or the 'shielding cutoff' wavelength.

For the NLC main damping ring, we find that perturbations with wavelengths $\lambda > 3.5$ mm are not stable due to the dipole CSR impedance alone. Adding the CSR impedance from the wiggler causes perturbations with wavelengths $\lambda > 2.6$ mm to be unstable. In Fig. 3, the threshold particle number is plotted as a function of the perturbation wavelength. Next, in Fig. 4, the growth rate, which is defined as the inverse of the time needed for the perturbation to grow by a factor of e

$$\frac{1}{\tau} \equiv \text{Im}(\Omega)ck|\eta|\nu_0 \ . \tag{11}$$

is plotted versus the perturbation wavelength. Based on the parameters in Table I and Eq. (10), the 'shielding cutoff' wavelength is computed to be $\lambda_c \approx 4.9$ mm. At this cutoff wavelength, the threshold currents and growth time are summarized in Table I. The growth time is significantly faster than the synchrotron period, in agreement with the analysis for a microwave-like instability.
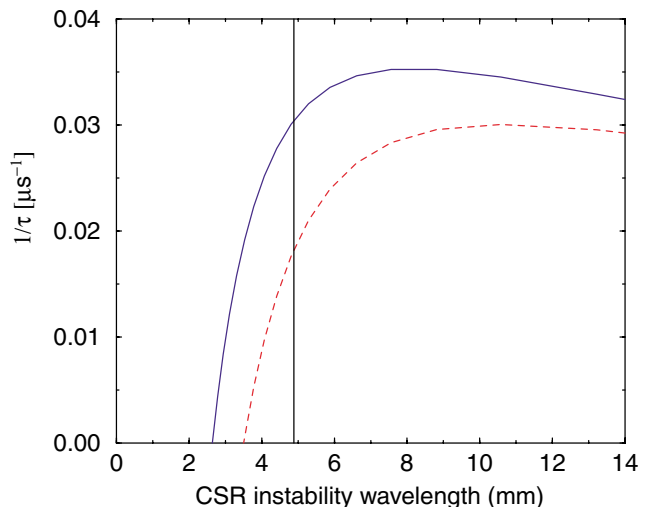

FIG. 4: The growth rate as a function of the CSR wavelength for the NLC main damping ring. The dashed curve is the result for the dipoles only, while the solid curve takes into account of the contributions from the dipoles and the wigglers. The vertical straight line is the approximate cutoff wavelength according to Eq. (10).
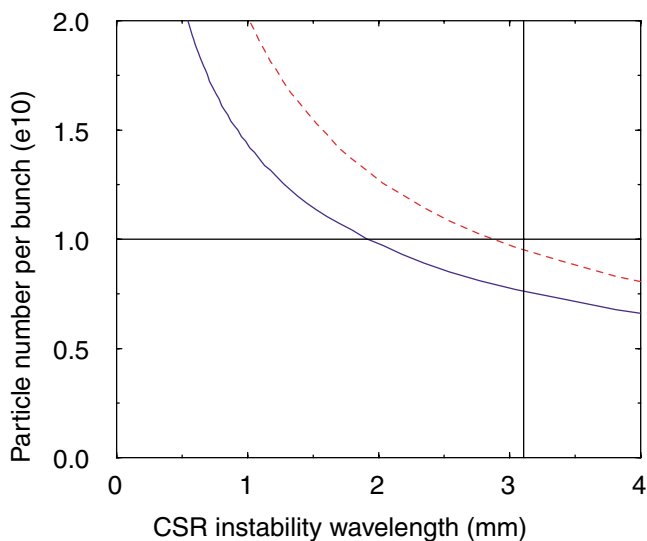
FIG. 5: The threshold particle number as a function of the CSR wavelength for the KEK ATF prototype damping ring. The dashed curve is the result for the dipoles only, while the solid curve takes into account of the contributions from the dipoles and the wigglers. The vertical straight line is the approximate cutoff wavelength according to Eq. (10). The horizontal straight line is the nominal number particles per bunch: 1.0×10^{10}.

It is clearly seen that the threshold current decreases as we approach the longer wavelength perturbations, however, the growth rate is not monotonic. This is the result of two opposite mechanisms: one is the energy modulation growth due to the CSR impedance, and the other is the Landau damping. For very long wavelength perturbation, Landau damping effect is small, hence, we could expand the denominator of the integrand in Eq. (4) to get

$$\omega = \sqrt{ic^2 n_b r_0 \eta k Z(k)/\gamma}, \qquad (12)$$

which indicates that $\tau^{-1} \propto \text{Im}(\omega) \propto \sqrt{kZ(k)}$, i.e., the growth rate will increase for a shorter wavelength perturbation, since $Z(k) \propto k^\varepsilon$, with $\varepsilon > 0$. This is shown in Fig. 4: when we approach from the long wavelength perturbation to the short wavelength perturbation, the growth rate increases.

However, this process stops when Landau damping becomes effective. The finite energy spread in the beam will produce a phase mixing due to the slippage and this will destroy density modulation due to the CSR induced energy modulation. The Landau damping due to the phase mixing is more serious for short wavelength perturbations. This damping can be seen in the second term of Eq. (1), or more clearly, in the denominator of the dispersion relation in Eq. (4). This is demonstrated in Fig. 4, the growth rate finally decreases when we approach very short wavelength, and eventually, the system becomes stable.

For the KEK ATF prototype damping ring, the cut-off

wavelength would be about $\lambda_c \approx 3.1$ mm according to Eq. (10). In Fig. 5, the threshold particle number is plotted as a function of the perturbation wavelength. Taking the dipole CSR impedance alone, for the single bunch charge, the instability sets in for perturbations with wavelengths $\lambda > 2.8$ mm. Adding the wiggler CSR impedance, the electron beam would be unstable for perturbations with wavelengths $\lambda > 1.9$ mm. Other results are summarized in Table I.

It is interesting to note that in both the NLC and the ATF damping rings roughly twice as much synchrotron radiation power is emitted in the wiggler as in the arc dipoles. However, the instability threshold is not dramatically impacted by the additional radiation in the wiggler and decreases by less than a factor of two in each case. This arises because of the very different low frequency behavior of the impedances.

We can use a simple scaling analysis to understand this. According to Eq. (7), the dipole CSR impedance scales as $Z_D(k) \propto k^{1/3}$. Similarly, the low frequency behavior of the wiggler impedance is [14]

$$Z_W(k) = \pi k_w \frac{k}{k_0} \left[1 - \frac{2i}{\pi} \log \left(\frac{k}{k_0} \right) \right] \qquad (13)$$

which is accurate enough for practical calculation in $k \in [0, 0.1\,k_0]$, where k_0 is the wiggler fundamental radiation wavenumber:

$$k_0 = 2\gamma^2 k_w / (1 + K^2/2) \qquad (14)$$

and the wiggler parameter K is approximately $K \approx 93.4\, B_w\, \lambda_w$, with B_w the peak magnetic field of the wiggler in units of Tesla and λ_w the period in meters. Thus, the wiggler CSR impedance scales as $\text{Re}(Z_W(k)) \propto k$, and $\text{Im}(Z_W(k)) \propto k \log(k)$, which have a weaker scaling than $Z_D(k) \propto k^{1/3}$ when $k \to 0$, i.e., the CSR impedance from the wiggler is weaker than that from the dipole when we approach low frequency region.

Hence, it suggests an optimization of the damping ring design where a larger fraction of radiation is emitted in the wigglers as will be discussed subsequently.

V. DAMPING RING OPTIMIZATION

Damping rings are used in linear colliders to attain the very small transverse emittances that required to attain the desired small spot sizes at the collision point. In the damping rings, the emission of synchrotron radiation damps the phase space volume of the injected beams towards the equilibrium values. An e-folding reduction of the transverse phase space occurs after the emission of synchrotron radiation energy comparable to the beam energy.

There are usually three conflicting requirements on the damping rings: first, the equilibrium emittances must be small which usually requires weak bends and strong focusing; second, the dynamic aperture must be large to

accept the injected beams and this is difficult to attain in a strong focusing storage ring; and, third, the damping rates must be fast so that the incoming phase space and transients can be damped before the beam are extracted and accelerated to the collision point.

To achieve these conflicting requirements most damping ring designs have been forced to include long damping wigglers where a significant fraction of the energy loss per turn is emitted. Of course, the ring characteristics can be greatly modified by changing the ratio of the damping due to the wiggler versus that due to the bending magnets. However, historically the wiggler systems have been a concern because they are a significant source of non-linearity and because they generate intense radiation which may directly or indirectly impact the beam.

Other work has improved the confidence in the dynamic aperture predictions and has shown that properly designed wigglers should not impose a limitation [24]. Thus, we can further optimize the ring designs based on quantitative evaluations of the effect of the wiggler radiation fields.

To study the ring optimization, we use expressions derived in Ref. [25] for the damping ring parameters. The primary constraint is the damping times. Because all linear collider designs presently only consider flat beams with $\sigma_x \gg \sigma_y$, the tightest requirement is on the vertical damping time which, using Eq. (11) of Ref. [25], can be written

$$\tau_y \approx \frac{(2.89 \times 10^{12} \text{kG})C}{|B_a|\gamma^2(1+F_w)c} \frac{|\Theta|}{2\pi} , \qquad (15)$$

where B_a is the arc bending field, C is the ring circumference, and Θ is the total bending angle of the arcs. In addition, F_w is a parameter equal to the ratio of the damping due to the wiggler over the damping due to the arc bending magnets which can be written:

$$F_w \equiv I_{2w}/I_{2a} . \qquad (16)$$

Here, I_{2a} and I_{2w} are the second synchrotron integrals calculated over the arcs and the wigglers respectively, which can be written

$$I_{2a} = \left| \frac{\Theta}{2\pi} \frac{2\pi B_a}{(B\rho)} \right| = \left| \frac{\Theta}{R} \right|; \qquad I_{2w} \approx \frac{L_w B_w^2}{2(B\rho)^2} . \qquad (17)$$

where $(B\rho)$ is the standard energy dependent magnetic rigidity, $(B\rho) \approx 0.017\gamma$ (kG m), and B_a, B_w, and L_w are the magnetic field of the bending dipole, the peak wiggler field, and the wiggler length.

According to Eq. (15), we can scale the bend field as

$$B_a \propto \frac{1}{(1+F_w)} \qquad (18)$$

for a given ring size and damping time and, given a maximum wiggler field, the required wiggler length can be found from Eqs. (17). At this point, we can calculate the other ring parameters. According to the dispersion relation in Eq. (6), we will need the momentum compaction factor α, the energy spread ν_0, and the bunch

rms length σ_z. Using Eqs. (37), (39) and (40) from Ref. [25], the scaling can be written:

$$\alpha \propto (1+F_w)^{5/3}; \qquad \nu_0 \propto \sqrt{\frac{B_a + B_w F_w}{1 + F_w}};$$

$$\sigma_z \propto \nu_0 \sqrt{\alpha} . \qquad (19)$$

Examples of the scaling of these parameters versus F_w can be found in Figs. 11 and 13 of Ref. [25] for an earlier version of the NLC damping ring. Using these relations, we estimated parameters for NLC ring with $F_w = 0$ and $F_w = 6.5$. These parameters are summarized in Table II along with the nominal parameters where $F_w = 2.2$.
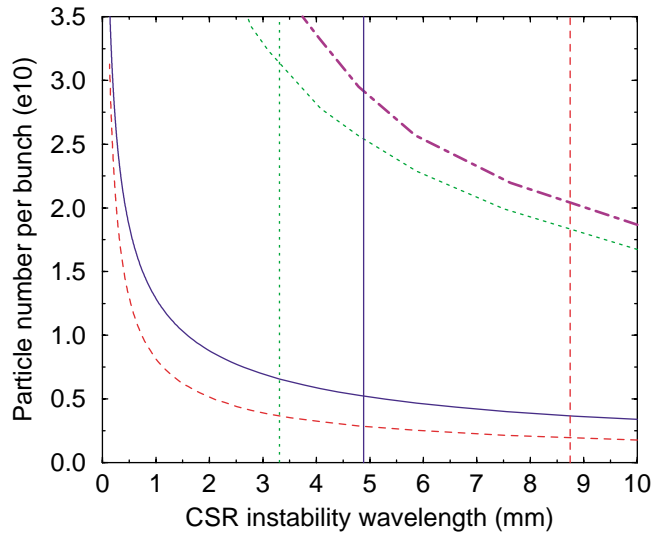

FIG. 6: The threshold particle number as a function of the CSR wavelength for the NLC main damping ring. The dashed curve is for $F_w = 0$ with the vertical dashed straight line indicating the corresponding cutoff wavelength. Their cross point gives the threshold at the cutoff wavelength. The solid curve and vertical solid straight line are for the case of $F_w = 2.2$, the nominal case in Table I. The dotted curve and vertical dotted straight line are for the case of $F_w = 6.5$. The dot-dashed curve is for the case of $F_w = 6.5$, but the impedance is the dipole CSR impedance alone.

At this point, we can calculate the impedance. Based on our previous studies, we expect the CSR impedance from the wiggler to be small compared to the CSR impedance of dipoles in the low frequency region of interest. Hence, the threshold is essentially determined by the dipole CSR impedance. According to the impedance in Eqs. (9) and (7), and the relation of B_a and F_w in Eq. (15), the total impedance should scale as

$$Z(k) \propto Z_D(k)R \propto R^{1/3} \propto (1+F_w)^{1/3} . \qquad (20)$$

at a fixed wavenumber k. Clearly, this is an increasing function with F_w however, according to the dispersion relation in Eq. (6), the threshold will scale as:

$$N_t \propto \frac{\alpha \nu_0^2 \sigma_z}{Z(k)} \propto (1+F_w)^{13/6} , \qquad (21)$$

F_w	0	2.2	6.5
Dipole field B_a/T	3.8	1.2	0.55
Dipole radius R/m	1.7	5.5	12.0
Wiggler length L_w/m	0	46.24	66
Momentum compaction $\alpha/10^{-4}$	0.69	2.95	14
Energy rms spread $\nu_0/10^{-4}$	13	9.09	8.4
Bunch rms length σ_z/mm	2.4	3.6	5.5
Cutoff wavelength λ_c/mm	8.7	4.9	3.3
Threshold at cutoff $N_t/10^9$	2.0	5.2	31.3

TABLE II: Parameters and results for the NLC main damping ring when F_w=0, 2.2 and 6.5 .

where it was assumed that $B_a \sim B_w$, so ν_0 is roughly constant. Thus, it is expected that increasing F_w will increase the threshold significantly.

In addition, the cutoff wavelength $\lambda_c \propto R^{-1/2} \propto B_a^{1/2} \propto (1 + F_w)^{-1/2}$. Hence, as F_w increases and B_a decreases, the cutoff wavelength will decrease. Since, the threshold is lowest at long wavelength, the threshold will increase as F_w is increased due to the shift in the cutoff wavelength as well as the change in the ring parameters.

The above scaling analysis has been compared to numerical calculations for the NLC damping ring. The results are given in Fig. 6 where we plot the threshold particle number as a function of the CSR instability wavelength for $F_w = 0$ (dashes), 2.2 (solid) and 6.5 (dots). In addition, the cutoff wavelength for the three cases is indicated with vertical lines using the same notation. Clearly, the threshold increases rapidly as F_w is increased as expected. The approximately quadratic scaling given above is followed as F_w is increased from the nominal value of 2.2 to 6.5 but the dependence is weaker as F_w is decreased to 0 because of the change in the beam energy spread which was assumed constant. Based on these results a new version of the NLC damping ring has been designed with an $F_w \approx 6.5$ which has a significantly higher threshold for both this CSR instability as well as the conventional microwave instability driven by the vacuum chamber impedance [26].

VI. DISCUSSION AND CONCLUSION

In this paper, we studied a possible beam instability due to coherent synchrotron radiation from dipole and wiggler magnets in a storage ring. This instability may be important in many high luminosity factories such as DAPHNE, PEP-II, KEK-B, and CESR-C as well as the damping rings of future linear colliders. We used the results to analyze the stability of the damping ring designs and found that a possible instability due to the CSR will exist in the NLC damping ring design and the ATF prototype damping ring at KEK. We then discuss

optimization of the rings and the pros and cons of increasing the damping fraction due to the wigglers. This led to a redesign for the NLC damping which increases the threshold to more than four times the nominal charge per bunch.

As we discussed above, in our calculation, we used steady state impedance for both the dipoles and wigglers. In the future, it may be important to consider transient effects in our calculation. In addition, the shielding cutoff of the CSR should be calculated as part of the impedance and not treated as an ad hoc limit. This is also important because we assumed the same shielding cutoff around the ring but in practice it will differ in the bending magnets and the wigglers. Finally, the bunch length is the same order of the instability wavelength, while in the theory, we use a coasting beam model. In the future, the finite bunch length should be taken into consideration. All of these topics are under study and will be reported in a separate paper.

APPENDIX A: GROWTH RATE AT THE FEL FREQUENCY AND THE ODD HARMONICS

In this appendix, we discuss the growth rates calculated at the wiggler fundamental frequency, frequently refered to as the FEL frequency, and at the odd harmonics. The wiggler CSR long-range wakefield is [14]

$$G(\zeta) = -\frac{1}{2\zeta} + \frac{1}{2\zeta} \sum_{n=0}^{\infty} \left[J_n\left(\frac{2n+1}{2}\right) - J_{n+1}\left(\frac{2n+1}{2}\right) \right]^2 \cos(4(2n+1)\zeta) \,. \tag{A1}$$

To the leading order in k, this gives us the CSR impedance as

$$
\begin{aligned}
Z(k) = {}& \pi k_w \frac{k}{k_0} \left\{ 1 - \sum_{n=0}^{\infty} \left(\left[J_n\left(\frac{2n+1}{2}\right) - J_{n+1}\left(\frac{2n+1}{2}\right) \right]^2 H[k - (2n+1)k_0] \right) \right\} - 2i k_w \frac{k}{k_0} \log\left(\frac{k}{k_0}\right) \\
& + \frac{1}{2} i k_w \frac{k}{k_0} \sum_{n=0}^{\infty} \left\{ \left[J_n\left(\frac{2n+1}{2}\right) - J_{n+1}\left(\frac{2n+1}{2}\right) \right]^2 \log\left(\frac{[k-(2n+1)k_0]^2[k+(2n+1)k_0]^2}{k_0^4}\right) \right\} \,, \tag{A2}
\end{aligned}
$$

where, $H(x)$ is the Heaviside step function, i.e., $H(x) = 1$ for $x > 0$, $H(0) = 1/2$, and $H(x) = 0$ for $x < 0$.

At the FEL frequency and the odd harmonics, the impedance has a logarithmically divergent imaginary part, $\mathrm{Im}(Z(k)) \propto \log(|\Delta k|/k)$, with $\Delta k \equiv k - (2n+1)k_0$, and the real part is finite. We write $Z = R - iL$, where $R > 0$ is the resistance and $L > 0$ is the inductance, and $L \gg R$. As a first estimate, we neglect the resistance and write $Z = -iL$ only. In the dispersion relation Eq. (6), then $|\Omega| \approx L \gg 1$. Now because of the factor $\exp(-p^2/2)$, Ω is huge compared with p in the p-nonvanishing integral region. Hence the integrand could be expanded. Keeping the first non-zero term, the integral is simplified as

$$\int_{-\infty}^{\infty} dp \, \frac{p \, e^{-\frac{p^2}{2}}}{\Omega \pm p} \approx \mp\sqrt{2\pi}\frac{1}{\Omega^2} \,, \tag{A3}$$

for large Ω to get

$$\Omega^2 = \pm\frac{L\,\Lambda}{k} \,. \tag{A4}$$

The upper (lower) sign in Eq. (A4) refers to the case of a positive (negative) η. For the rings which we study in this paper, they all have $\eta > 0$ and we take the upper sign. Hence, $\mathrm{Im}(\Omega) = 0$, i.e., the growth rate will be zero and the system is stable at the FEL frequency and all the odd harmonics. This agrees with the conventional knowledge that a ring is stable with a purely inductive impedance and a positive momentum compaction or a purely capacitive impedance and a negative momentum compaction.

APPENDIX B: SINGLE WIGGLER

In this appendix, we study the beam instability in a single wiggler. From FEL theory, we would expect in-
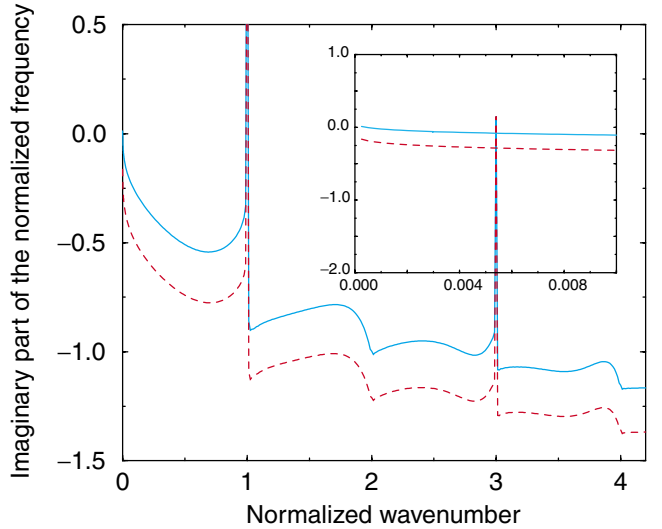

FIG. 7: The imaginary part of the normalized frequency Ω as a function of the normalized wavenumber k/k_0 where k_0 is the on-axis wiggler fundamental radiation wavenumber. The solid curve is for the wigglers in the NLC main damping ring and the dashed curve is for the TESLA damping ring.

stability at the wiggler fundamental radiation frequency and all the harmonics. In addition, we need to look at a microwave-like low-frequency instability.

In a wiggler, the slippage factor is

$$\eta = -\frac{\left(1 + \frac{K^2}{2}\right)}{\gamma^2} \,. \tag{B1}$$

i.e., the slippage factor is negative, therefore, we choose the lower $(-)$ sign in Eq. (6). In Fig. 7, we plot the imaginary part of Ω as a function of the instability wave

number for the wigglers in the NLC and TESLA damping rings [16, 17]. For the region where $\text{Im}(\Omega) < 0$, the beam is stable. We find that, for the nominal current, the system is stable within the entire interesting region where the perturbation wavelength $\lambda < 3$ cm, except at the wiggler fundamental radiation wavelength and the third harmonic.

In fact, according to Eq. (B1), we have $\eta < 0$ and we need take the lower sign in Eq. (A4). When we approach the fundamental and the third harmonic frequency, L becomes large, and Eq. (A4) gives us a large $\text{Im}(\Omega)$, i.e., a large growth rate as we find in Fig. 7. However, according to Eq. (A4), we will have $\text{Im}(\Omega) \propto I^{1/2}$, where I is the peak current of the electron bunch; while in the FEL theory, the growth rate scales as $\text{Im}(\Omega) \propto I^{1/3}$ [19]. To correctly calculate the FEL instability from the wake impedance approach, the electron density distribution function has to be taken at the retarded time in the standard Vlasov equation [20]. This then leads to a cubic dispersion relation same as in the FEL theory, and results in the cubic root scaling in the growth rate:

$$\text{Im}(\Omega) \propto I^{1/3}.$$

Nevertheless, here we further use the FEL theory to study the instability at the FEL frequency and the third harmonic. We use the simulation code TDA [21] to calculate the instability growth length at the fundamental frequency and a newly developed code [22] to calculate the instability at the third harmonic. The wiggler and beam parameters used are listed in Table I. In the NLC damping wiggler, the growth length at the FEL frequency is about 50 m assuming that the phase errors between wiggler sections is small. Fortunately, the separation between the 2-meter long wiggler sections will further reduce the gain. In addition, any modulation that is induced at the fundamental wavelength of $\sim 10\,\mu\text{m}$ will be smeared out by the energy spread and the momentum compaction as the beam is transported around the remainder of the ring. A similar conclusion is found for the TESLA damping ring wigglers and the instability at the FEL frequency and the odd harmonics are not expected to be a limitation in either case.

[1] J.B. Murphy, S. Krinsky, and R.L. Gluckstern, Part. Accel. **57**, 9 (1997); J.B. Murphy, S. Krinsky, and R.L. Gluckstern, in *Proceedings of the 1995 IEEE Particle Accelerator Conference* (IEEE, Piscataway, NJ, 1996), p. 2980; A. Faltens and L.J. Laslett, Part. Accel. **4**, 152 (1973).

[2] Ya.S. Derbenev *et al.*, DESY Report No. DESY-TESLA-FEL-95-05, 1995.

[3] R. Warnock, P. Morton, Part. Accel. **25**, 113 (1990); R. Warnock, SLAC Report: SLAC-PUB-5417, 1991; SLAC-PUB-5523, 1991.

[4] K.Y. Ng, Part. Accel. **25**, 153 (1990).

[5] H. Braun, F. Chautard, R. Corsini, T.O. Raubenheimer, P. Tenenbaum, Phys. Rev. Lett. **84**, 658 (2000).

[6] H. Braun, R. Corsini, L. Groening, F. Zhou, A. Kabel, T.O. Raubenheimer, R. Li, T. Limberg, Phys. Rev. ST Accel. Beams **3**, 124402 (2000).

[7] M. Hüning, P. Piot and H. Schlarb, Nucl. Instrum. Meth. A **475**, 348 (2001).

[8] M. Borland and J. Lewellen, in *Proceedings of the 2001 IEEE Particle Accelerator Conference* (IEEE, Piscataway, NJ, 2002), p. 2839.

[9] G. Stupakov, S. Heifets, Phys. Rev. ST Accel. Beams **5**, 054402 (2002).

[10] G. Vignola [DAPHNE project team Collaboration], LNF-91-037-R *Presented at Workshop on Physics and Detectors for DAPHNE, Frascati, Italy, Apr 9-12, 1991.*

[11] PEP-II: An Asymmetric B-factory, SLAC-418 (1993).

[12] KEK Report 95-7 (1995).

[13] G. Dugan *et al.*, in *Proc. of the APS/DPF/DPB Summer Study on the Future of Particle Physics (Snowmass 2001)* ed. N. Graf, eConf **C010630**, T201 (2001).

[14] J. Wu, T.O. Raubenheimer, G.V. Stupakov, Phys. Rev. ST Accel. Beams **6**, 040701 (2003).

[15] E.L. Saldin, E.A. Schneidmiller, and M.V. Yurkov, Nucl. Instrum. Methods Phys. Res., Sect. A **417**, 158 (1998).

[16] A. Wolski, "NLC Damping Rings: Lattice Parameters, Information and Resources", (URL: http://awolski.lbl.gov/nlcdrlattice/default.htm).

[17] W. Decking, "Damping Ring Lattice Update", talk given at the *TTF Collaboration Meeting*, DESY, 7-9 July 1999; "The TESLA Damping Ring", talk given at the *Snowmass 2001*, July 2001.

[18] http://www-jlc.kek.jp/atf/ATF.overview-e.html .

[19] R. Bonifacio, C. Pellegrini, L. Narducci, Opt. Commun., **50**, 373 (1984).

[20] G. Stupakov and S. Krinsky, "Derivation of FEL gain using wakefield approach," submitted to 2003 Part. Acc. Conference, Portland, Oregon (2003).

[21] T.M. Tran, J.S. Wurtele, Comput. Phys. Commun. **54**, 263 (1989).

[22] J. Wu, "Harmonic contents of and detailed study on a High-Gain Harmonic Generation Free Electron Laser," submitted to 2003 Part. Acc. Conference, Portland, Oregon (2003).

[23] G.V. Stupakov, I.A. Kotelnikov, Phys. Rev. ST Accel. Beams **6**, 034401 (2003).

[24] M. Venturini, "Wigglers and Single-Particle Dynamics in the NLC Damping Rings," submitted to 2003 Part. Acc. Conference, Portland, Oregon (2003).

[25] P. Emma, T. Raubenheimer, Phys. Rev. ST Accel. Beams **4**, 021001 (2001).

[26] A. Wolski *et al.*, "A Lattice With Large Momentum Compaction for the NLC Main Damping Rings," submitted to 2003 Part. Acc. Conference, Portland, Oregon (2003).